Pharmacologically inducing regenerative cardiac cells by small molecule drugs

Wei Zhou[1,2,†], Kezhang He[2,†], Chiyin Wang[3], Pengqi Wang[2], Dan Wang[2], Bowen Wang[1,2], Han Geng[2], Hong Lian[3], Tianhua Ma[2]*, Yu Nie[3]*, Sheng Ding[1,2,4]*

Affiliations

[1]Tsinghua-Peking Joint Center for Life Sciences, Tsinghua University, Beijing 100084, China

[2]School of Pharmaceutical Sciences, Tsinghua University, Beijing 100084, China

[3]State Key Laboratory of Cardiovascular Disease, Fuwai Hospital, National Center for Cardiovascular Disease, Chinese Academy of Medical Sciences and Peking Union Medical College, Beijing, 100037, China

[†]W.Z. and K.Z.H. contributed equally to this work.

[4]Lead contact

*Corresponding author. Email: matianhua@tsinghua.edu.cn (T.M.), nieyu@fuwaihospital.org (Y.N.), shengding@tsinghua.edu.cn (S.D.)

Summary

In contrast to lower organisms, adult mammals cannot regenerate damaged hearts through de-differentiation of cardiomyocytes (CMs) into cells with regenerative capacity. Development of an enabling condition to induce such naturally unavailable cells with potential to proliferate and differentiate into CMs, i.e., regenerative cardiac cells (RCCs), in mammals will provide new insights and tools for heart regeneration. Here, a two-compound combination (2C), CHIR99021 and A-485, was identified to robustly induce RCCs from human embryonic stem cell (hESC) derived TNNT2^{+} CMs *in vitro*, which was confirmed by lineage tracing experiments. Functional analyses revealed that RCCs expressed a spectrum of genes essential for cardiogenesis and exhibited potential to become functional CMs, endothelial cells (ECs) and smooth muscle cells (SMCs). Consistent with the results in human cells, 2C-induced generation of RCCs were also observed in neonatal rats CMs *in vitro* and *in vivo*. Remarkably, administration of 2C can induce RCCs in adult mouse hearts and significantly improve survival and heart function in the mice undergoing myocardial infarction. Mechanistically, CHIR99021 is indispensable for transcriptional and epigenetic activation of genes essential for RCC, whereas A-485 mainly function to epigenetically down-regulate H3K27Ac and particularly H3K9Ac in CMs. Their combination specifically enhances both H3K27Ac and H3K9Ac on RCC genes, facilitating the establishment of RCC state dedifferentiated from CMs. Therefore, our findings demonstrated the feasibility and revealed the mechanisms of pharmacological induction of RCCs from endogenous CMs, which could offer a promising regenerative strategy to repair injured hearts.

Main Text

Lower organisms, such as zebrafish, possesses a robust cardiac regeneration capacity through CM dedifferentiation characterized by reactivation of embryonic cardiogenic genes and disassembly of their sarcomeric structures (Kikuchi & Poss, 2010; Lepilina *et al*, 2006). In contrast, limited cardiac regeneration was only permitted from postnatal day 1 to day 6 (PN1 to PN6) in mice with sarcomeric disassembly and proliferation of CMs in the resected section of heart (Porrello *et al*, 2011), which is no longer observed beyond this narrow time window. Therefore, discovery of small molecule drugs enabling induction of regenerative capacity in mammalian adult endogenous CMs by recapitulating the regenerative cellular state presented in zebrafish will shed mechanistic lights on the understanding of roadblocks preventing CMs from dedifferentiation in mammalian hearts, and facilitate development of regenerative medicine to treat various heart diseases caused by CM loss.

During mammalian heart development, cardiomyocytes (CMs) mainly originate from first heart field (FHF) and second heart field (SHF) (Srivastava, 2006). In particular, SHF cells marked by the pioneer transcription factor ISL1 can proliferate and differentiate into three major cardiovascular cell types, CMs, SMCs and ECs during embryonic heart development (Bu *et al*, 2009; Moretti *et al*, 2006). Consistently, a small number of ISL1^{+} cells residing in the neonatal mouse heart between postnatal Day 1 and Day 5 were reported to expand and differentiate into CMs under appropriate *in vitro* conditions (Laugwitz, 2005). Since ISL1 transcriptionally governs the expression of a cohort of cardiac genes, e.g., *NKX2-5* (Ma *et al*, 2008), *FGF10* (Watanabe *et al*, 2012), essential for embryonic cardiogenesis, it is reasonable to hypothesize that induced expression of ISL1 in CM may be a determinative step in the induction of regenerative cardiac cells (RCCs).

Toward induction of regeneration capacity in CMs, we conducted a screening for small molecules that can induce the expression of ISL1 in CMs. Our combinatorial screening identified a novel combination of CHIR99021 and A-485/2C that could unprecedentedly and efficiently induce dedifferentiation of human CMs into RCCs. These RCCs exhibited disassembled sarcomeric structures, high expression of embryonic cardiogenic genes, and increased number of CMs through re-differentiation *in vitro*. Further studies showed that 2C could robustly generate RCCs in hearts of adult mice and improve cardiac function in the mice with myocardial infarction. Our proof-of-concept discovery demonstrated that a simple combination of small molecule drugs can grant regenerative capacity to the heart by reprogramming CMs into RCCs.

2C treatment efficiently induces dedifferentiation of hESC-derived CMs

To obtain an adequate number of CMs for small molecule screening, we differentiated hESCs into CMs (*SI Appendix,* Fig. S1*A* and Movie S1) following a well-established step-wise protocol (Lian *et al*, 2013). Consistent with previous reports, nearly homogenous contracting CMs were observed on day 10 of differentiation. After purification with glucose-depleted medium containing abundant lactate (*SI Appendix,* Fig. S1*B*), highly pure TNNT2^{+} CMs were obtained, and then subsequently dissociated and seeded into 96-well plates. When CMs resumed contraction, they were treated with individual small molecules from a

collection of over 4,000 compounds for 3 days (*SI Appendix,* Fig. S1*C* and Table S1), and then fixed and immunostained with ISL1. Using a high-content imaging (HCI) and analysis system, five compounds were initially identified to potentially induce regenerative capacity in CMs, indicated by induced sarcomere disassembly and ISL1 expression (*SI Appendix,* Fig. S1*D*). After further comparing the effects from various combinations, the unique combination of CHIR99021 and A-485 (2C) was found to most efficiently induce ISL1 expression with healthy cell state (*SI Appendix,* Fig. S1*E*).

When CMs with well-organized sarcomeres were treated with 2C *in vitro*, cells started to exhibit dedifferentiation-associated phenotype, such as reduction of cell size after 24 hours and growing as clusters after 48 hours and forming colonies after 60 hours (Fig. 1*A* and *SI Appendix,* Fig. S2 *A-C*). During this time, the expression of TNNT2 and MYL2 were gradually downregulated while ISL1 expression and the percentage of $ISL1^+$ cells were gradually increased (*SI Appendix,* Fig. S2 *D-G*). Compared to untreated CMs, significant sarcomere disassembly and reduction of cytoplasmic/nuclear area were observed in cells treated with 2C for 60 hours (Fig. 1 B-D). In parallel, the number and percentage of $TNNT2^+$ cells remained constant while $ISL1^+$ cells increased remarkably (Fig. 1 *E-G*), accompanied by a ~3-fold increase ISL1 expression at both mRNA and protein levels (Fig. 1 *H-J*). Of note, other typical genes involved in early embryonic cardiogenesis, including MESP1, LEF1 (Klaus *et al*, 2007), FUT4 (Wang *et al*, 2019), and NR2F2 (Churko *et al*, 2018) were also induced by 2C to express at high levels (Fig. 1*J* and *SI Appendix,* Fig. S2*H*). In addition, treatment with 2C resulted in significantly decreased expression of CM-specific genes, such as TNNT2, MYL2, MYL7, and MEF2C, while the pan-cardiac transcription factors, GATA4, TBX5, and NKX2-5, showed no obvious expression changes (Fig. 1*J* and *SI Appendix,* Fig. S2*H*). Furthermore, when we generated mature CMs from hESCs by treating differentiating cells with ZLN005 following a previously reported method (Liu *et al*, 2020), 2C could induce ISL1 expression in these mature CMs (*SI Appendix,* Fig. S2*I*). These results suggested that CMs might be converted by 2C into a state with regenerative capacity.

2C induced cells possess regenerative capacity

To confirm the regenerative capacity of 2C-induced cardiac cells, we investigated cell proliferation using a BrdU incorporation assay. Immunostaining clearly showed the co-localization of ISL1 and BrdU labeling in cells (Fig. 2*A*), and subsequent statistical analysis revealed a significant decrease in the nuclear area and increase in the cell percentage of $ISL1^+/BrdU^+$ positive cells following 2C treatment (Fig. 2 *B* and *C*). We next examined the potential for re-differentiation of 2C-induced cardiac cells into CMs. As expected, upon withdrawal of 2C and subsequent culture in CM media for 3 days (60h+3d), we observed the emergence of spontaneously contracting cells exhibiting CM-specific morphology with typical size of cytoplasmic/nuclear area (Fig. 2 *D-F* and Movie S2), downregulated expression of early embryonic cardiogenesis genes and upregulated expression of CM-specific genes, and the expression of pan-cardiac genes didn't show any noticeable changes throughout this process (*SI Appendix,* Fig. S3*A*). Remarkably, there was a 1.4-fold increase in the number of re-differentiated CMs with clear TNNT2 staining relative to the initial CMs before 2C treatment (Fig. 2 *G* and *H*), demonstrating a regenerative potential in 2C-induced cardiac cells. In addition to CMs, 2C-induced cardiac cells were capable of differentiation towards SMA^+

SMCs or CD31$^+$/VE-Cadherin$^+$ ECs in the presence of PDGF-BB and TGF-β1 or VEGF, bFGF and BMP4, respectively (Fig. 2*I* and *SI Appendix,* Fig. S3 *B-D*). In contrast, the expression of those genes was not detectable in DMSO-treated cells. Collectively, our findings indicate that treatment with 2C facilitates the conversion of CMs into cardiac cells with regenerative capability, including proliferative potential and ability to differentiate into the three major cardiovascular cell types, which were therefore named as regenerative cardiac cells (RCCs).

Lineage tracing demonstrated that 2C induced RCCs dedifferentiated from TNNT2$^+$ CMs

Although TNNT2$^+$ CMs purified by lactate-based culture medium were almost homogeneous populations, we noticed that these were still a low percentage (<4%) of purified cells still expressed ISL1 (*SI Appendix,* Fig. S1*B*). Therefore, we performed lineage-tracing experiments to further confirm that the 2C-induced RCCs were actually dedifferentiated from TNNT2$^+$ CMs rather than proliferation of those residual ISL1$^+$ cells. Upon directed cardiac differentiation of an ISL1$^{mCherry/+}$ H9 hESC (K9) line established through CRISPR-based knock-in (*SI Appendix,* Fig. S4 *A-D*), mCherry expression faithfully reflected endogenous ISL1 expression (Fig. 3 *A-C*). After purification of K9-derived CMs, mCherry-negative cells were selected by FACS (Fig. 3 *D* and *E*), all of which were confirmed to be TNNT2$^+$ CMs (*SI Appendix,* Fig. S4*E*). Those mCherry-negative CMs were then treated with 2C for 60 hours. The expression of TNNT2 and MYL2 were dramatically down-regulated, whereas the expression of ISL1 and mCherry was significantly up-regulated (Fig. 3 *F* and *K*). We found the induced mCherry$^+$/ISL1$^+$ RCCs exhibited significant morphological changes accompanied by a dramatic decrease in TNNT2 expression (Fig. 3*F*). In contrast, the mCherry-negative CMs remained high expression of TNNT2 with the typical sarcomere structure (Fig. 3*F*). FACS analysis further confirmed that 2C was capable of K9-derived mCherry-negative CMs into mCherry$^+$/ISL1$^+$ cells (Fig. 3 *G* and *H*). Consistently, similar results were observed using HUES7 hESC line with ISL1-mCherry knock-in reporter (K7) (Fig. 3 *I*, *J*, *L*, and *SI Appendix,* Fig. S5).

Furthermore, we used a lineage-tracing system to unequivocally examine the conversion of CMs to ISL1-expressing RCCs by 2C treatment. In this assay, CMs were transfected with plasmids encoding CreERT2 under the control of TNNT2 promoter and an EGFP reporter following flox-stop-flox cassette (*SI Appendix,* Fig. S6*A*). After optimizing virus titer and infection time (*SI Appendix,* Fig. S6 *B-D*), ~0.6 of K9-derived mCherry-negative CMs were permanently labeled with EGFP following 6 days of treatment with tamoxifen (Fig. 3 *M* and *N*). Then, those EGFP-labeled mCherry-negative CMs were sorted by flow cytometry and subsequently treated with 2C for 60 hours. As expected, the expression of ISL1 was observed in these EGFP$^+$ CMs (Fig. 3*O*). Collectively, these results robustly demonstrated that RCCs with ISL1 expression were truly generated by 2C treatment from TNNT2$^+$ CMs.

2C-induced dedifferentiation of CMs provided a protective effect on cardiac infarction

In order to examine 2C's reprogramming effect on CMs *in vivo*, we first tested 2C on primary neonatal rat CMs (Sakurai *et al*, 2014), on which 2C was found to consistently induce RCCs generation with corresponding ISL1 induction and morphological changes (*SI Appendix,* Fig. S7*A*). Then, we sought to

examine whether 2C was capable of reprograming endogenous CMs to RCCs *in vivo*. For this purpose, neonatal SD rats were intraperitoneally administrated with 20 mg/kg of CHIR99021 and 10 mg/kg of A-485 daily for 5 days (*SI Appendix,* Fig. S7*B*). Compared to the vehicle/DMSO controls (NC), ISL1 was robustly induced in the cells from hearts of rats treated with 2C without apparent effects on body weight (*SI Appendix,* Fig. S7 *C* and *D*). These induced ISL1-expressing cells were widely distributed within the region 600 µm to 3000 µm down from the base of the hearts, including aorta (Ao), left/right atria, and both ventricles (*SI Appendix,* Fig. S7*E*). Notably, all of these $ISL1^+$ expressed TNNT2 as well, strongly indicating 2C-induced RCCs were actually originated from CMs *in vivo*. More importantly, neither administration of 20 mg/kg CHIR99021 nor 10 mg/kg A-485 alone observed $ISL1^+$ cells in ventricles, powerfully illustrating the combined effect of 2C on the induction of RCCs (*SI Appendix,* Fig. S8).

Similarly, RCCs were also efficiently induced in the Ao root and RA regions of the heart dissected from adult 129SvJ mice administrated with 2C (20 mg/kg of CHIR99021 and 10 mg/kg of A-485) for 5 consecutive days as well (Fig. 4*A*). Intriguingly, we sought to explore whether 2C-induced RCCs could rescue cardiac function in mice subjected to myocardial infarction (MI). In a prophylactic setting, mice were pre-treated with either 2C or vehicle/DMSO for 5 days (Fig. 4*B*) and then inducing MI by ligation of left anterior descending (LAD) artery. When measuring cardiac function with magnetic resonance imaging (MRI) on days 1, 8, 25 and 35 post-MI, we found pretreatment with 2C was able to significantly improve both cardiac function and survival rate in the mice, without affecting their body weight (Fig. 4 *C*-*E*). Next, when we treated mice with 2C or vehicle/DMSO post-MI in a therapeutic setting (Fig. 4*F*), remarkably mice with 2C treatment displayed a recovered cardiac function as assessed by both left ventricular ejection fraction (LVEF) and echocardiography (Fig. 4 *G* and *H*). Consistently, cardiac fibrosis was largely ameliorated in 2C-treated mice that displayed significantly smaller scar size in the hearts compared to control mice (Fig. 4*I*). Those *in vivo* studies collectively indicate that 2C or further improved small molecule drugs with similar mechanisms may have therapeutic utility to repair or regenerate hearts after cardiac injury. Altogether, these *in vivo* studies indicate that 2C-induced RCCs possess the same regenerative capacities comparable to those generated *in vitro,* which will shed light on development of small molecule drugs with therapeutic utility to repair or regenerate hearts after cardiac injury.

Both CHIR99021 and A-485 are required to induce dedifferentiation of CMs to RCCs

To gain insights into mechanisms involved in 2C-induced dedifferentiation of CMs to RCCs, we performed bulk RNA-seq analysis of K9-derived ISL1/mCherry-negative CMs treated with DMSO (NC) or 2C for 60 hours (Fig. 5*A*). Analysis of differentially expressed genes (DEGs) revealed a remarkable change in the transcriptome upon 2C treatment (Fig. 5*B*). In detail, 2C treatment led to increased expression of a large set of genes known to be associated with embryonic cardiogenic genes (e.g., MSX1, BMP4, TCF4, and LEF1) and suppression of a significant list of genes associated with CMs (Fig. 5*C*). Consistently, gene ontology (GO) analysis further revealed that down-regulated genes were mainly involved in cardiac maturation and muscle contraction (Fig. 5*D*), while up-regulated genes were enriched in cell junction and catenin complex (Fig. 5 *E* and *F*). Those embryonic cardiogenic genes and other genes significantly up-

regulated (e.g., MSX2, NKD1, PDGFC, CTNNA2) after 2C treatment were confirmed by qPCR in K9-derived mCherry-negative CMs (Fig. 5*G*).

To investigate the individual effects of CHIR99021 and A-485 on induction of RCCs, we compared H9 hESC-derived CMs treated with CHIR99021 and A-485 individually or in combination. When measuring cytoplasmic/nuclear area, we found CHIR99021 significantly reduced both cytoplasmic and nuclear area, a distinguishable morphological feature of RCCs, in comparison to A-485 that only reduced cytoplasmic area (*SI Appendix,* Fig. S9 *A*-*C*). Consistently, disassembly of sarcomere structures was more frequently observed in CMs treated with CHIR99021 than in CMs treated with A-485 (*SI Appendix,* Fig. S9*E*). Although reduced expression of TNNT2 and MYL2 as well as increased expression of ISL1 can be induced individually by CHIR99021 and A-458 (*SI Appendix,* Fig. S9 *D* and *E*), CHIR99021 was able to uniquely promote the expression of a cohort of genes involved in embryonic cardiogenesis, including BMP4, NKD1, MSX2, PDGFC, LEF1 and TCF4 (*SI Appendix,* Fig. S9*D*). Upon withdrawal of CHIR99021, A-485 or 2C, the cell percentage of $ISL1^+$ cell was similarly and significantly reduced (*SI Appendix,* Fig. S9*F*). Of note, a drastic increase in the number of $TNNT2^+$ CMs was only observed in redifferentiation of 2C-treated cells, as confirmed by statistical analysis (*SI Appendix,* Fig. S9*G*). These findings suggested that CHIR99021 played a leading role in 2C-induced de-differentiation of CMs to RCCs, A-485 is also indispensable.

Reprogramming of CMs to RCCs by 2C went through an intermediate cell state

Next, we performed scRNA-seq of K9-derived mCherry-negative CMs treated with DMSO (NC) or 2C for 60 hours. Utilizing UMAP analysis, we observed the proportion of cells within three (cluster 0, 2, 3) out of 7 identified clusters increased after 2C treatment (Fig. 6 *A* and *B*). Among these three clusters, cells in cluster 2 highly expressed RCC characteristic genes, including those essential for embryonic cardiogenesis (*e.g.,* ISL1, BMP4 and FGF20 (a key gene involved in expansion of early embryonic progenitor cells (Cohen *et al*, 2007)), and cell proliferation marker gene MKI67 (Fig. 6 *C* and *D*). By contrast, cells in cluster 0, 3, 4, and 5 expressed CMs specific markers (*e.g.,* MYH6 and MYL2) at high levels (Fig. 6 *C* and *D*), indicating they were CMs. Meanwhile, cells in cluster 1 and 6 were considered as intermediate cells (ICs) during 2C-induced reprogramming of CMs to RCCs, because of expression of ACTA2, a marker gene reported to express in CM dedifferentiation, and genes associated with CM development, including COL1A1, COL1A2, and COL3A1 (Cui *et al*, 2020; Mononen *et al*, 2020) (Fig. 6 *C* and *D*).

When further examining cluster 2 with 435 cells from DMSO-treated cells and 410 cells from 2C-treated cells by second-level clustering analysis, we identified subcluster 0 (408, or 48.3% out of 845 cells) in cluster 2 which was exclusively observed in 2C-treated cells (Fig. 6 *E and F*). Furthermore, cells in subcluster 0 expressed a series of RCC-related genes essential for embryonic cardiogenesis, including MSX1, LEF1, BMP4, MSX2, and HAND1 (Fig. 6*G*), as well as a series of genes co-expressed with ISL1 in SHF progenitors *in vivo*, such as NR2F2, TBX5, ALCAM (Ghazizadeh *et al*, 2018), and CXCR4 (Andersen *et al*, 2018) (Fig. 6*G*), strongly indicating cells in subcluster 0 represent RCCs induced by 2C treatment. Thus, a unique gene set that included LIX1, NKD1, PDGFC, ARL4A, AXIN2, FZD7, ISL1, MSX1, MSX2, BMP4, LEF1, and HAND1 was found to determine RCC state during the reprogramming of CMs by 2C, and

hence designated as RCC genes. In addition, the pseudo-time analysis that clearly revealed 2C-induced reprogramming of CMs (highly expressing TNNT2) went through ICs (highly expressing COL1A1), and ultimately towards RCCs (highly expressing ISL1 and FGF20) (Fig. 6 *H-I*).

RCC and CM genes were epigenetically regulated by 2C during reprogramming of CMs into RCCs

As a p300 acetyltransferase inhibitor, A-485 was previously reported to specifically inhibit acetylation of H3 at lysine 27 (H3K27Ac) but not at lysine 9 (H3K9Ac) in the PC3 cells (Lasko *et al*, 2017). Consistently, the percentage of H3K27Ac$^+$ cells but not that of H3K9Ac$^+$ cells were specifically and significantly reduced in CMs were treated with A-485 alone (*SI Appendix,* Fig. S10). In contrast, neither CHIR99021 nor 2C treatment resulted in noticeable alterations in the percentage of H3K27Ac$^+$ and H3K9Ac$^+$ cells (*SI Appendix,* Fig. S10). Intriguingly, further analyses revealed a remarkable reduction in the levels of H3K27Ac and H3K9Ac in TNNT2$^+$ cells following A-485 treatment (*SI Appendix,* Fig. S10 *F* and *L*), suggesting that A-485 simultaneously inhibit both H3K27Ac and H3K9Ac on CM-specific genes during the dedifferentiation of CMs.

To gain more insights on the mechanism underlying 2C-induced silencing of CM genes and activation of RCC genes during reprogramming of CMs to RCCs, we performed chromatin immunoprecipitation-sequencing (ChIP-seq) analyses of H3K27Ac and H3K9Ac in DMSO, A-485, CHIR99021 and 2C-treated H9 hESC-derived CMs (Fig. 7*A*). We identified active promoters as proximal regions (±4 kb from the transcription start sites, or TSS) exhibiting H3K4me3 enrichment in the cells treated with DMSO or 2C (Fig. 7 *B*, and *C*). Treatment with 2C led to a striking increase in H3K9Ac and H3K27Ac enrichment around TSS regions on a whole-genome-wide scale (Fig. 7 *B* and *C*). Consistently, 2C treatment induced a significantly enhanced enrichment of H3K9Ac in 4,485 genes and H3K27Ac enrichment in 2,560 genes, whereas a decreased of H3K9Ac and H3K27Ac enrichment was detected in 346 and 1,834 genes respectively (*SI Appendix,* Fig. S11 *A-F*). Of note, a significant part of genes decreased H3K9Ac (268, or 58.1% out of 461) and H3K27Ac (777, or 68.6% out of 1132) enrichment in A485-treated cells were also observed among genes that H3K9Ac (268, or 77.5% out of 346) and H3K27Ac (777, or 42.4% out of 1834) enrichment following 2C treatment. Further GO analysis revealed that those genes decreased H3K9Ac and H3K27Ac enrichment in their promoters commonly seen in repose to A-485 or 2C treatment, preferentially exhibited cardiac specific functions, such as cardiac muscle contraction, sarcomere organization, and heart contraction (*SI Appendix,* Fig. S11 *G-L*). Compared to individual treatment with A-485 or CHIR99021, 2C treatment resulted in an increased H3K9Ac and H3K27Ac enrichment in the genes associated with cell cycle and cell division (*SI Appendix,* Fig. S11 *K* and *L*), strongly supporting the combined effects of 2C on RCC cell state establishment.

Next, we specifically examined H3K9Ac and H3K27Ac peaks in the promoters of critical CM genes and RCC genes in the cells treated with or without A-485, CHIR99021 or 2C. We observed that both A-485 and CHIR99021 effectively reduced the peaks of H3K9Ac and H3K27Ac in the promoters of CM genes, including TNNT2, TNNI1, MYL7, MYH6, and MYH7. These reductions were further intensified with 2C treatment (Fig. 7*D and SI Appendix,* Fig. S12*A*). Interestingly, increased peaks of H3K9Ac and H3K27Ac in promoters of the RCC genes, such as LEF1, AXIN2, BMP4, LIX1, MSX1, MSX2, and NKD1, was only

observed in condition with CHIR99021 available (Fig. 7*D and SI Appendix,* Fig. S12*B*). Other RCC genes, including ISL1, ARL4A, FZD7, HAND1, and PDGFC, exhibited a significantly elevated peaks of H3K9Ac and H3K27Ac by treatment with 2C and much higher than those treated with CHIR99021 alone (Fig. 7*D and SI Appendix,* Fig. S12*C*). Therefore, while CHIR99021 was able to activate the expression of RCC genes and simultaneously repressed CM genes partially through changing H3K27Ac and H3K9Ac during 2C-induced CM dedifferentiation to RCC, A-485 can inhibit CM genes directly through reducing of H3K27Ac and H3K9Ac modifications in the promoters of CM-specific genes, thereby assisting CHIR99021 to establish RCC state.

In addition, we observed that different small molecules had varied impacts on distribution of H3K9Ac and H3K27Ac enrichment during 2C-induced dedifferentiation of CM into RCC. As indicated by Veen diagram, distributions of H3K9Ac and H3K27Ac enrichment significantly diverged among cells treated with DMSO, A-485, CHIR99021, and 2C (Fig. 7 *E* and *F*). For genes with H3K9Ac enrichment, 2716 (or 46.1%) out of 5891 annotated genes were only enriched in the cells treated with 2C, while only 527 (or 4.9%) out of 10785 annotated genes with H3K27Ac enrichment was exclusively observed (Fig. 7 *E* and *F*). Thus, the process of 2C-induced dedifferentiation of CM to RCC is accompanied by vigorous alterations in H3K9Ac, whereas H3K27Ac is remain relatively stable, indicating that the genome-wide distribution of H3K9Ac exhibited drastic distinction between CMs and RCCs. To further confirm this notion, we performed a comparative analysis of annotated genes between the cells treat with 2C or DMSO to validate the most significant differential genes (i.e., Log10LR>3) under the respective condition. In comparison to 430 genes with H3K9Ac enrichment observed in DMSO-treated cells, which were mainly involved in cardiac muscle contraction (Fig. 7 *G* and *H*), 2C treatment markedly enhanced the enrichment of H3K9Ac in 123 genes associated with the transcription factor complex and Wnt signaling pathway (Fig. 7 *I* and *J*). In particular, 12 CM genes, including TNNT2, were ranked in top 90 out of 430 annotated genes with H3K9Ac enrichment. In contrast, 7 RCC genes, including ISL1, were ranked in the top 50 out of 123 annotated genes with H3K9Ac enrichment. Moreover, DNA-binding motif analysis indicated that the ISL1 binding motifs only exhibited accessibility in the cells treated with A-485 or 2C (Fig. 7*K*), underscoring the vital role of A-485 in 2C treatment to activate the expression of RCC genes. Taken together, these findings revealed that CHIR99021 is responsive for transcriptional and epigenetic activation of genes essential for cardiac embryonic development, while A-485 promotes conversion of CMs to RCCs by epigenetic downregulation of H3K27Ac and particularly H3K9Ac in CMs, which together facilitate the induction of RCCs from CMs.

Discussion

It is worth noting that the RCCs were only generated in hearts of 2C-treated postnatal rats, but not in rats after treatment with only 20 mg/kg CHIR99021 or 10 mg/kg A-485 alone (*SI Appendix,* Fig. S8), indicating the reprogramming of endogenous CMs to RCCs depends on the cooperative effect from these two molecules. CHIR99021 has been well characterized as a GSK3 inhibitor to activate the Wnt signaling pathway. Previous studies have elucidated the role of CHIR99021 in initiating proliferation of hPSC-derived CMs (Buikema *et al*, 2020; Quaife-Ryan *et al*, 2020), accompanied by induction of H3K27Ac on promoter

regions of multiple cardiac lineage genes, including TNNT2, MYH6, and ISL1 (Quaife-Ryan *et al.*, 2020). However, this proliferation was only achieved in neonatal CMs *in vivo* (Buikema *et al.*, 2020; Quaife-Ryan *et al.*, 2020). Consistently, we also found the enhanced levels of H3K27Ac in TNNT2$^+$ CMs by treatment with CHIR99021 alone or 2C (Fig. 7*D* and *SI Appendix,* Fig. S10*F*). In addition, we found that the p300/CBP inhibitor A-485 facilitate the reprogramming of CMs into RCCs by epigenetically inhibiting expression of CM-specific genes such as TNNT2 (Fig. 7*D* and *SI Appendix,* Fig. S9*D*), while enhancing the modifications of H3K9Ac and H3K27Ac on RCC-specific genes such as ISL1 in combination with CHIR99021 (Fig. 7 *D* and *K*). These findings promoted us to postulate that A-485 and its mediated mechanism may be used to modulate the cell fate of other terminally differentiated cells by epigenetically suppressing the expression of corresponding lineages specific genes.

2C-induced RCCs exhibited potential to differentiate into three cardiac-lineages of the heart *in vitro*, which might contribute additional beneficial effects in heart repair and regeneration. Furthermore, RCCs expressed a broad set of genes essential for embryonic cardiogenesis (Fig. 1*J* and Fig. 5*G*), including ISL1, and a series of potentially important genes identified in this study (Fig. 6*G*), all of which were highly expressed in ISL1$^+$ SHF cardiac progenitors during mammalian heart development. However, RCCs had a restricted proliferation capacity, although they were able to be passaged 3-5 times under 2C conditions (data not shown), which is distinct to ISL1$^+$ cardiac progenitors (Bu *et al.*, 2009; Moretti *et al.*, 2006). These findings collectively indicated that 2C-induced RCCs dedifferentiated from CMs may be expandable under an appropriate condition and deserve further investigation.

References

1. Andersen P, Tampakakis E, Jimenez DV, Kannan S, Miyamoto M, Shin HK, Saberi A, Murphy S, Sulistio E, Chelko SP *et al* (2018) Precardiac organoids form two heart fields via Bmp/Wnt signaling. *Nat Commun* 9: 3140
2. Bu L, Jiang X, Martin-Puig S, Caron L, Zhu S, Shao Y, Roberts DJ, Huang PL, Domian IJ, Chien KR (2009) Human ISL1 heart progenitors generate diverse multipotent cardiovascular cell lineages. *Nature* 460: 113-117
3. Buikema JW, Lee S, Goodyer WR, Maas RG, Chirikian O, Li G, Miao Y, Paige SL, Lee D, Wu H *et al* (2020) Wnt Activation and Reduced Cell-Cell Contact Synergistically Induce Massive Expansion of Functional Human iPSC-Derived Cardiomyocytes. *Cell Stem Cell* 27: 50-63 e55
4. Churko JM, Garg P, Treutlein B, Venkatasubramanian M, Wu H, Lee J, Wessells QN, Chen SY, Chen WY, Chetal K *et al* (2018) Defining human cardiac transcription factor hierarchies using integrated single-cell heterogeneity analysis. *Nat Commun* 9: 4906
5. Cohen ED, Wang Z, Lepore JJ, Lu MM, Taketo MM, Epstein DJ, Morrisey EE (2007) Wnt/beta-catenin signaling promotes expansion of Isl-1-positive cardiac progenitor cells through regulation of FGF signaling. *J Clin Invest* 117: 1794-1804
6. Cui M, Wang Z, Chen K, Shah AM, Tan W, Duan L, Sanchez-Ortiz E, Li H, Xu L, Liu N *et al* (2020) Dynamic Transcriptional Responses to Injury of Regenerative and Non-regenerative Cardiomyocytes Revealed by Single-Nucleus RNA Sequencing. *Developmental Cell* 53: 102-116.e108
7. Ghazizadeh Z, Fattahi F, Mirzaei M, Bayersaikhan D, Lee J, Chae S, Hwang D, Byun K, Tabar MS, Taleahmad S *et al* (2018) Prospective Isolation of ISL1(+) Cardiac Progenitors from Human ESCs for Myocardial Infarction Therapy. *Stem Cell Reports* 10: 848-859
8. Kikuchi K, Poss KD (2010) Primary contribution to zebrafish heart regeneration by gata4(+) cardiomyocytes. *Nature* 464: 601-605
9. Klaus A, Saga Y, Taketo MM, Tzahor E, Birchmeier W (2007) Distinct roles of Wnt/beta-catenin and Bmp signaling during early cardiogenesis. *Proc Natl Acad Sci U S A* 104: 18531-18536
10. Lasko LM, Jakob CG, Edalji RP, Qiu W, Montgomery D, Digiammarino EL, Hansen TM, Risi RM, Frey R, Manaves V *et al* (2017) Discovery of a selective catalytic p300/CBP inhibitor that targets lineage-specific tumours. *Nature* 550: 128-132
11. Laugwitz K-L (2005) Postnatal isl1 cardioblasts enter fully differentiated cardiomyocyte lineages. *Nature*
12. Lepilina A, Coon AN, Kikuchi K, Holdway JE, Roberts RW, Burns CG, Poss KD (2006) A dynamic epicardial injury response supports progenitor cell activity during zebrafish heart regeneration. *Cell* 127: 607-619
13. Lian X, Zhang J, Azarin SM, Zhu K, Hazeltine LB, Bao X, Hsiao C, Kamp TJ, Palecek SP (2013) Directed cardiomyocyte differentiation from human pluripotent stem cells by modulating Wnt/beta-catenin signaling under fully defined conditions. *Nat Protoc* 8: 162-175
14. Liu Y, Bai H, Guo F, Thai PN, Luo X, Zhang P, Yang C, Feng X, Zhu D, Guo J *et al* (2020) PGC-1alpha activator ZLN005 promotes maturation of cardiomyocytes derived from human embryonic stem cells. *Aging (Albany NY)* 12: 7411-7430
15. Ma Q, Zhou B, Pu WT (2008) Reassessment of Isl1 and Nkx2-5 cardiac fate maps using a Gata4-based reporter of Cre activity. *Dev Biol* 323: 98-104
16. Mononen MM, Leung CY, Xu J, Chien KR (2020) Trajectory mapping of human embryonic stem cell cardiogenesis reveals lineage branch points and an ISL1 progenitor-derived cardiac fibroblast lineage. *Stem Cells*
17. Moretti A, Caron L, Nakano A, Lam JT, Bernshausen A, Chen Y, Qyang Y, Bu L, Sasaki M, Martin-Puig S *et al* (2006) Multipotent embryonic isl1+ progenitor cells lead to cardiac, smooth muscle, and endothelial cell diversification. *Cell* 127: 1151-1165
18. Porrello ER, Mahmoud AI, Simpson E, Hill JA, Richardson JA, Olson EN, Sadek HA (2011) Transient regenerative potential of the neonatal mouse heart. *Science* 331: 1078-1080
19. Quaife-Ryan GA, Mills RJ, Lavers G, Voges HK, Vivien CJ, Elliott DA, Ramialison M, Hudson JE, Porrello ER (2020) beta-Catenin drives distinct transcriptional networks in proliferative and nonproliferative cardiomyocytes. *Development* 147
20. Sakurai T, Lanahan A, Woolls MJ, Li N, Tirziu D, Murakami M (2014) Live cell imaging of primary rat neonatal cardiomyocytes following adenoviral and lentiviral transduction using confocal spinning disk microscopy. *J Vis Exp*: e51666

21. Srivastava D (2006) Making or breaking the heart: from lineage determination to morphogenesis. *Cell* 126: 1037-1048
22. Wang J, Liu M, Wu Q, Li Q, Gao L, Jiang Y, Deng B, Huang W, Bi W, Chen Z *et al* (2019) Human Embryonic Stem Cell-Derived Cardiovascular Progenitors Repair Infarcted Hearts Through Modulation of Macrophages via Activation of Signal Transducer and Activator of Transcription 6. *Antioxid Redox Signal* 31: 369-386
23. Watanabe Y, Zaffran S, Kuroiwa A, Higuchi H, Ogura T, Harvey RP, Kelly RG, Buckingham M (2012) Fibroblast growth factor 10 gene regulation in the second heart field by Tbx1, Nkx2-5, and Islet1 reveals a genetic switch for down-regulation in the myocardium. *Proc Natl Acad Sci U S A* 109: 18273-18280

Acknowledgments

This work is supported by the National Natural Science Foundation of China (32030031 to S.D.), Beijing Natural Science Foundation (JQ22016 to T.M.), the National Key R&D Program of China (2022YFA1103704 to S.D.; 2022YFA1104503 to Y. N.), Center for Life Sciences (to S.D.).

We thank the Center for Pharmaceutical Technology, Tsinghua University for the activity screening platform, Biomarker Technologies Corporation, Beijing, China and BeiJing Geek Gene Technology Co Ltd for technical support, and support from Tsinghua-Peking Center for Life Sciences.

Author Contributions

Conceptualization, S.D. and W.Z.; Methodology, W.Z., H.L., T.H.M. and Y.N.; Investigation, W.Z., C.Y.W., K.Z.H., P.Q.W., B.W.W., and H.G.; Visualization, W.Z., P.Q.W., B.W.W., H.G., and D.W.; Funding Acquisition, S.D., T.H.M., and Y.N.; Project Administration, W.Z., H.L., T.H.M., and Y.N.; Supervision: S.D., and W.Z.; Writing – Original Draft, W.Z., T.H.M., and S.D.; Writing – Review & Editing: W.Z., T.H.M., Y.N., S.D.

Competing Interests

The authors declare no competing interests.

Data and Materials availability

All targeted amplicon sequencing data have been deposited in the Sequence Read Archive of the NCBI under the BioProject accession number PRJNA903530. All data are available in the main text or the supplementary materials.

Figure and Figure legends

Fig. 1. 2C treatment induced dedifferentiation of hESC-derived CMs toward ISL1-expressing cells. Cells induced from hESC-derived CMs by treatment with DMSO (NC) or 2C for 60 hours. **A,** Phase contrast images showing cell morphology. **B,** Immunofluorescence staining of the ISL1 (ISL1, green), and the CM marker cardiac troponin T (TNNT2, red) in the cells. Nuclei were stained by DAPI (4′,6-diamidino-2-phenylindole) and presented in DNA blue. **(C** and **D)**, Cytosolic (**C**) and nuclear (**D**) areas of the cells. **E**, The number of total cells, TNNT2+ cells, and ISL1$^+$ cells. **F**, Cell percentage of TNNT2$^+$ cells. **G**, Fraction of ISL1$^+$ cell in TNNT2$^+$ cells. Error bars represent SD. ns, not significant (P > 0.05); **P < 0.01; ***P < 0.001. (**H** and **I)** Western blot (**H**) and quantitative analysis (**I**) of ISL1 expression in DMSO (NC) or 2C-treated CMs for 60 hours. Error bars represent SD. *P < 0.05; **J**, Heatmap illustration showing the fold-changes of indicted marker genes' expression by 2C treatment, which were measured using qRT-PCR.

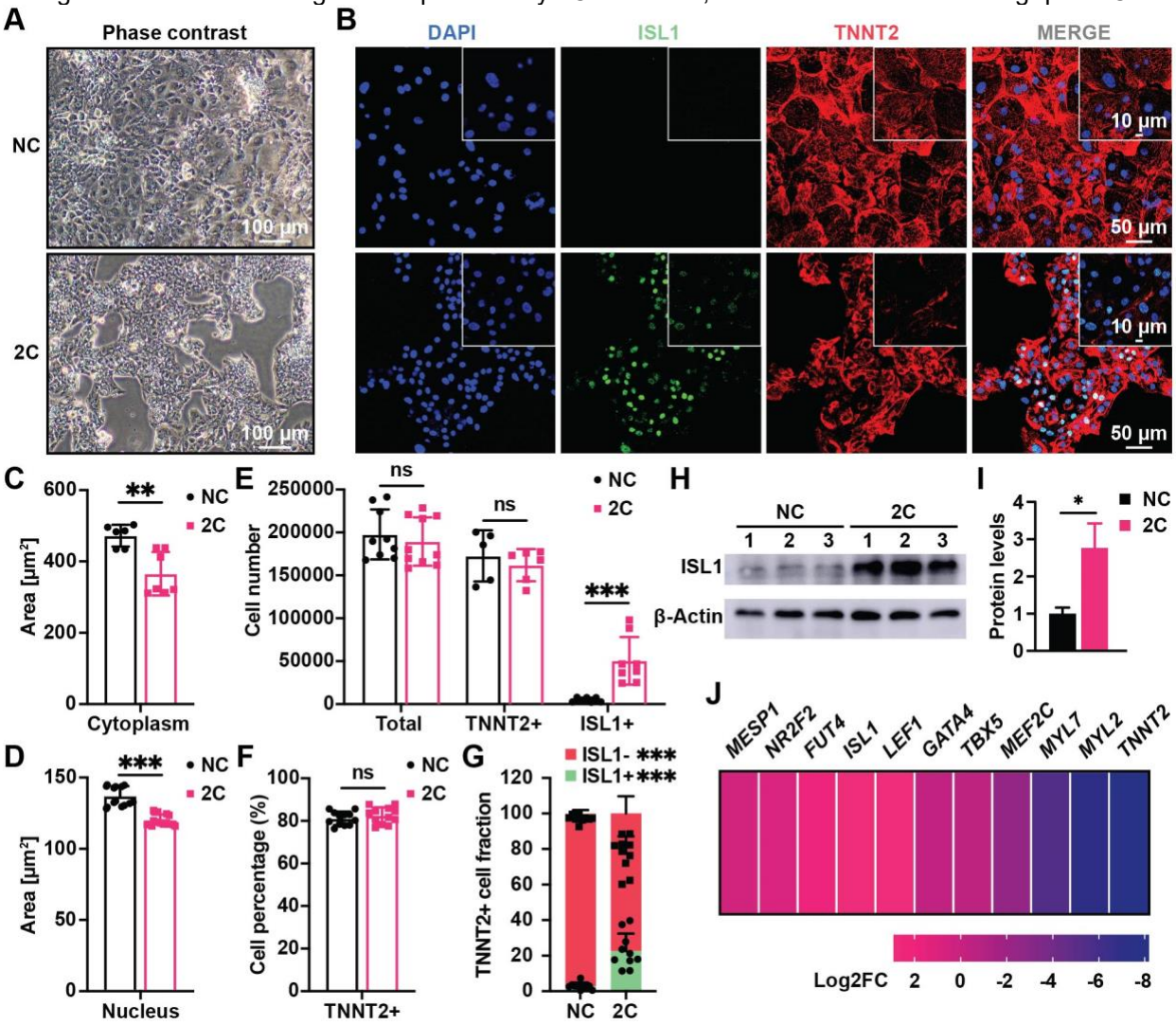

Fig. 2. Regenerative ability of 2C-induced RCCs. (**A**-**C**)**,** Immunofluorescence staining (**A**) and statistical analysis (**B** and **C**) of the ISL1 (green) and BrdU (red) double positive RCCs induced from CMs by treatment with DMSO (NC) or 2C for 60 hours. DAPI (4′,6-diamidino-2-phenylindole) staining labeled nuclei as blue. Error bars represent SD. **P < 0.01. **D,** Phase contrast images of hESC-derived CMs treated by DMSO (NC) or 2C for 60 hours (60h) and subsequently cultured in the absence of 2C for another 3 days (60h+3d). (**E** and **F),** Cytosolic (**E**) and nuclear (**F**) areas of the cells under the same condition in (**D**). Error bars indicate SD. ns, not significant (P > 0.05); ***P < 0.001. **G,** Immunostaining showed the expression of ISL1 (green) and TNNT2 (red) in the cells under the same condition in (**D**). **H,** The fold change of $TNNT2^+$ cells under the same condition in (**D**). Error bars represent SD. ns, not significant (P > 0.05); **P < 0.01. Immunostaining showed the expression of EC markers (CD31, green and CD144, red), SMC marker (SMA, red), and CM marker (TNNT2, green).

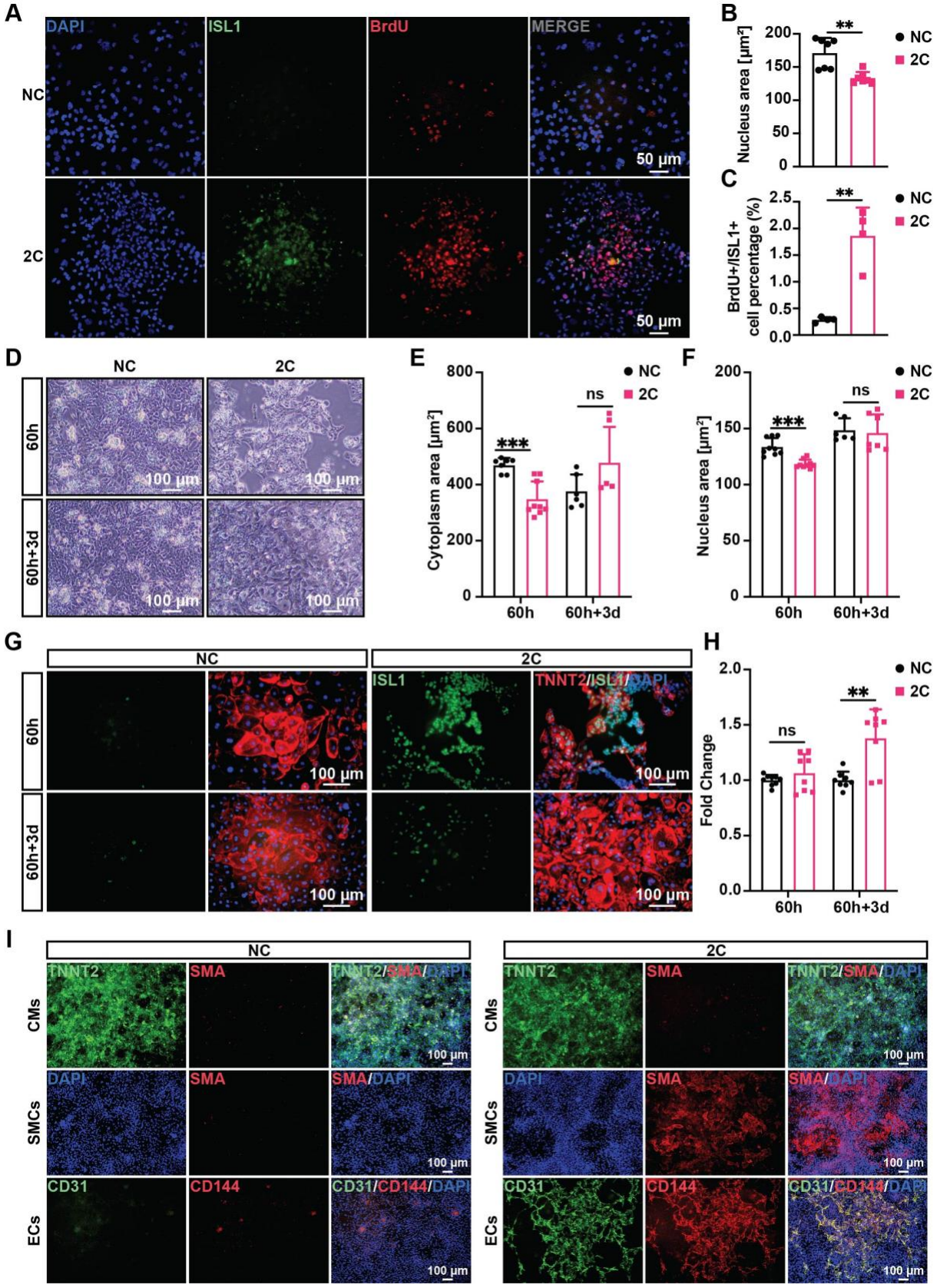
A
DAPI
ISL1
BrdU
MERGE
NC
2C
50 μm
B
Nucleus area [μm²]
**
NC
2C
C
BrdU+/ISL1+ cell percentage (%)
**
D
NC
2C
60h
60h+3d
100 μm
E
Cytoplasm area [μm²]
***
ns
60h
60h+3d
F
Nucleus area [μm²]
***
ns
G
ISL1
TNNT2/ISL1/DAPI
H
Fold Change
ns
**
I
CMs
SMCs
ECs
TNNT2
SMA
TNNT2/SMA/DAPI
DAPI
SMA/DAPI
CD31
CD144
CD31/CD144/DAPI

418

Fig. 3. Lineage tracing demonstrated 2C induced dedifferentiation of TNNT2+ CMs to ISL1-expressing RCCs. A, Immunofluorescence images showing expression of endogenous ISL1 (green) and ISL1-mCherry (red) reporter in the cells differentiated from K9 hESC KI reporter line at day 6 (D6). (**B** and **C**) Flow cytometry analysis of the percentage of mCherry^{+}/ISL1^{+} cells in the cells differentiated from K9 at D6. (**D** and **E**) Flow cytometry analysis of the percentage of mCherry-negative cells at selection day 4 (SD4) in lactate purification medium. Error bars represent SD. (**F**-**H**) Cells induced from mCherry-negative CMs by treatment with or without 2C for 60 hours. Images showing the expression of mCHERRY (red) and TNNT2 (green) in the cells (**F**) and flow cytometry analysis of the percentage of mCherry-positive cells (**G** and **H**). Error bars represent SD. (**I** and **J**) Flow cytometry analysis of the percentage of mCherry-positive cells dedifferentiated from K7 hESC KI reporter line derived mCherry-negative CMs. Error bars represent SD. **(K** and **L),** Relative gene expression of ISL1, mCHERRY, LEF1, TNNT2 and MYL2 in K9- and K7-derived mCherry-negative CMs treated with DMSO (NC) or 2C for 60 hours, respectively. Error bars represent SD. *P < 0.05; **P < 0.01; ***P < 0.001. (**M** and **N)** Flow cytometric plots showing EGFP-labeled CMs by lineage-tracing of K9-derived mCherry-negative CMs (**M**), and bar graph showing the percentage of mCherry-negative CMs expressing EGFP (**N**). Error bars represent SD. **O,** Images showing the expression of ISL1 (red) and EGFP (green) in the cells induced from EGFP-positive/mCherry-negative CMs in (**M**) by treatment with or without 2C for 60 hours.

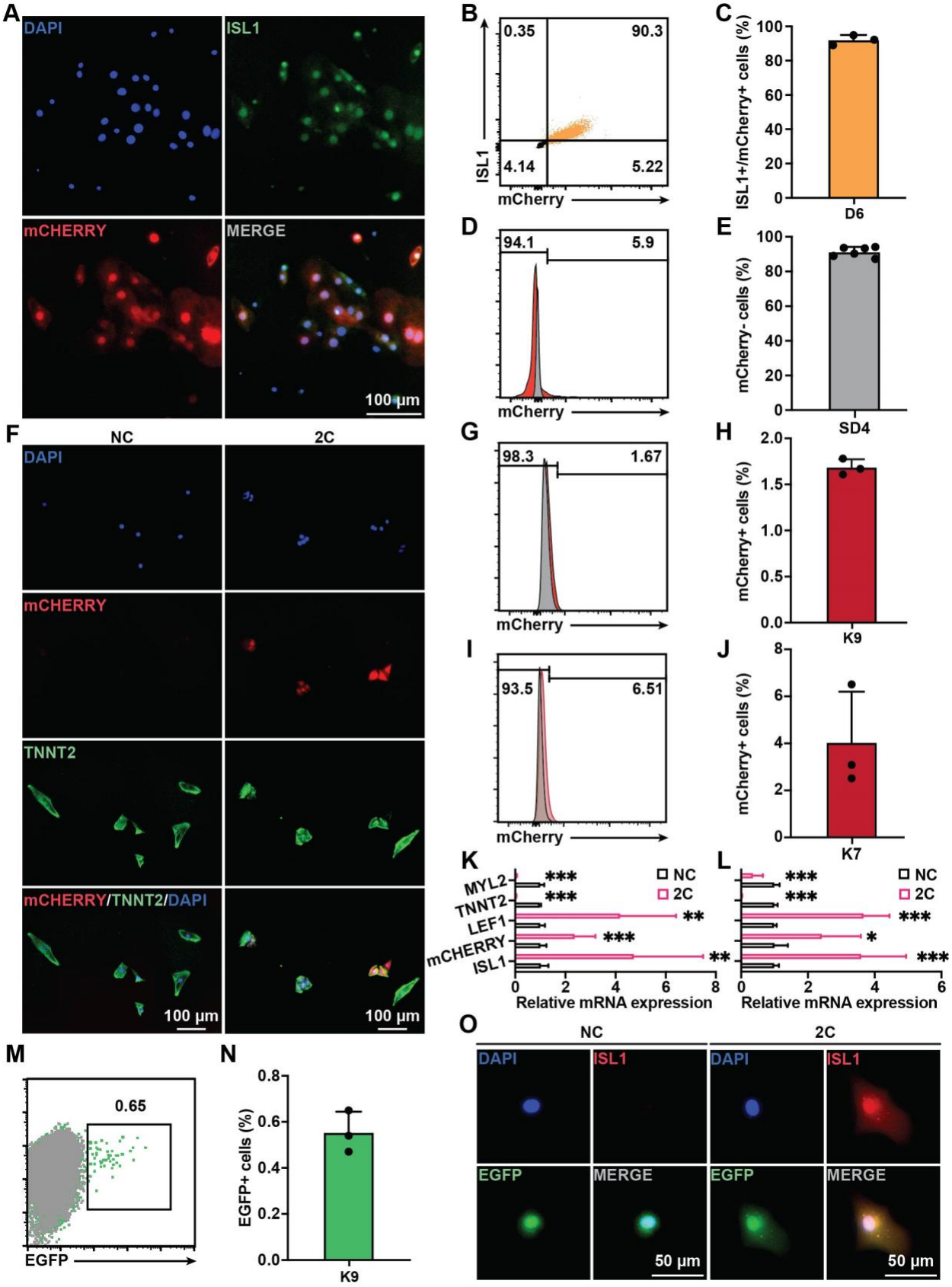
A
DAPI
ISL1
mCHERRY
MERGE
100 μm
B
0.35
90.3
4.14
5.22
ISL1
mCherry
C
ISL1+/mCherry+ cells (%)
D6
D
94.1
5.9
mCherry
E
mCherry- cells (%)
SD4
F
NC
2C
DAPI
mCHERRY
TNNT2
mCHERRY/TNNT2/DAPI
100 μm
G
98.3
1.67
mCherry
H
mCherry+ cells (%)
K9
I
93.5
6.51
mCherry
J
mCherry+ cells (%)
K7
K
MYL2
TNNT2
LEF1
mCHERRY
ISL1
NC
2C
Relative mRNA expression
L
Relative mRNA expression
M
0.65
EGFP
N
EGFP+ cells (%)
K9
O
NC
2C
DAPI
ISL1
EGFP
MERGE
50 μm

Fig. 4. Heart regeneration *via* 2C-induced dedifferentiation of CMs. A, Immunofluorescence staining of ISL1 (green) and TNNT2 (red) in cross-sectioned hearts from 2C or vehicle-treated (NC) adult 129SvJ mice. Ao, aorta. PA, pulmonary artery. LA, left atrial. RA, right atrial. IAS, interatrial septum. **B,** Schematic illustration of the method used to examine the prophylactic effect of 2C in 129SvJ mice post MI. **C,** Body weight of mice pre-treated with vehicle (DMSO) or 2C as shown in (**B**) at Day 12, Day 16, Day20, and Day35 after MI (1dpi). Error bars represent SD. ns, not significant ($P > 0.05$). **D,** Survival curve of sham-operated mice and mice pre-treated with vehicle (DMSO) or 2C as shown in (**B**), at indicated time points before or after MI. **E,** Ejection fraction (EF) of sham-operated mice and mice pre-treated with vehicle (DMSO) or 2C as shown in (**B**), before MI (baseline) or at Day 1, Day8, Day25, and Day35 after MI (1dpi). Error bars represent SD. ns, not significant ($P > 0.05$); **$P < 0.01$; ***$P < 0.001$. **F,** Schematic illustration of the method used to examine therapeutic effect of 2C in the 129SvJ mice post MI. **G,** Echocardiography of sham-operated mice and mice treated with vehicle (DMSO) or 2C as shown in (**F**) at Day 35 post MI. **H,** Serial fMRI measurements showing the cardiac function from sham-operated mice and mice treated with vehicle (DMSO) or 2C at as shown in (**F**), at Day 35 post MI. Error bars represent SD. *$P < 0.05$. **I,** Masson staining of serial transverse sections of hearts from sham-operated mice and mice treated with vehicle (DMSO) or 2C as shown in (**F**), at Day 35 post MI.

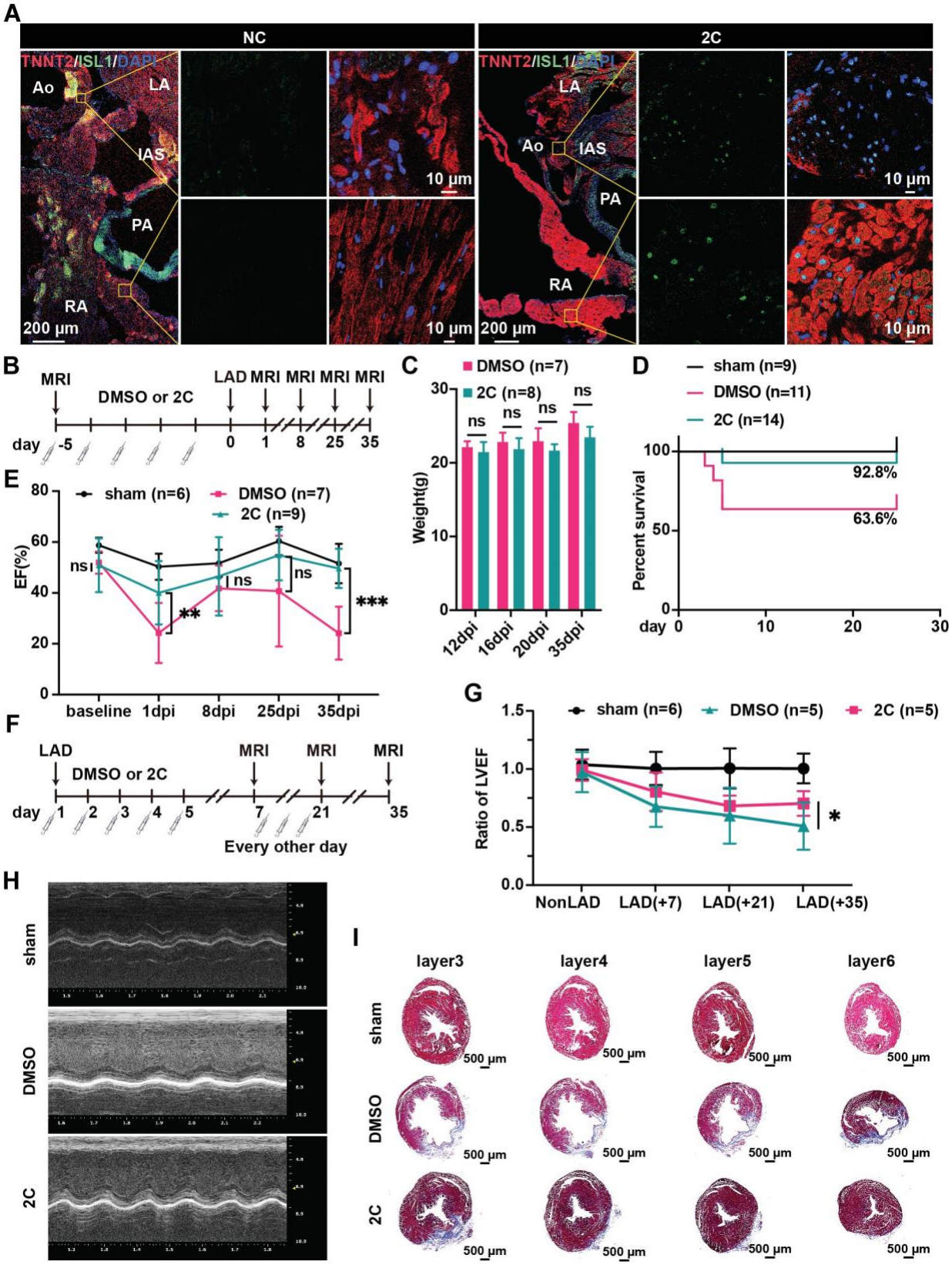
A
NC
2C
TNNT2/ISL1/DAPI
Ao
LA
IAS
PA
RA
200 μm
10 μm
B
MRI
DMSO or 2C
LAD MRI MRI MRI MRI
day -5 0 1 8 25 35
C
DMSO (n=7)
2C (n=8)
Weight(g)
ns
12dpi 16dpi 20dpi 35dpi
D
sham (n=9)
DMSO (n=11)
2C (n=14)
Percent survival
92.8%
63.6%
day 0 10 20 30
E
sham (n=6)
DMSO (n=7)
2C (n=9)
EF(%)
ns
**
***
baseline 1dpi 8dpi 25dpi 35dpi
F
LAD
DMSO or 2C
MRI MRI MRI
day 1 2 3 4 5 7 21 35
Every other day
G
sham (n=6)
DMSO (n=5)
2C (n=5)
Ratio of LVEF
*
NonLAD LAD(+7) LAD(+21) LAD(+35)
H
sham
DMSO
2C
I
layer3
layer4
layer5
layer6
sham
DMSO
2C
500 μm

455

Fig. 5. Bulk RNA-seq of analysis of 2C-treated ISL1/mCherry-negative CMs. A, Scheme of bulk RNA-seq analysis of K9-derived mCherry-negative CMs with DMSO (NC) or 2C treatment for 60 hours. **B,** Heatmap of differentially expressed genes (DEGs) in ISL1/mCherry-negative CMs treated with DMSO (NC) or 2C for 60 hours. **C**, Volcano plot showing genes significantly changed by 60 hours of 2C treatment. (**D** and **E**) Gene Ontology (GO) analysis of downregulated (**D**) and upregulated (**E**) genes in ISL1/mCherry-negative CMs by 2C treatment for 60 hours, compared to DMSO (NC) treated cells. **F,** Plotting GO terms of upregulated genes by 2C treatment with cnetlpot. **G,** Relative expression fold-changes of indicated genes in K9-derived ISL1/mCherry-negative CMs by 60 hours of DMSO (NC) or 2C treatment. Error bars indicate SD. **P < 0.01; ***P < 0.001.

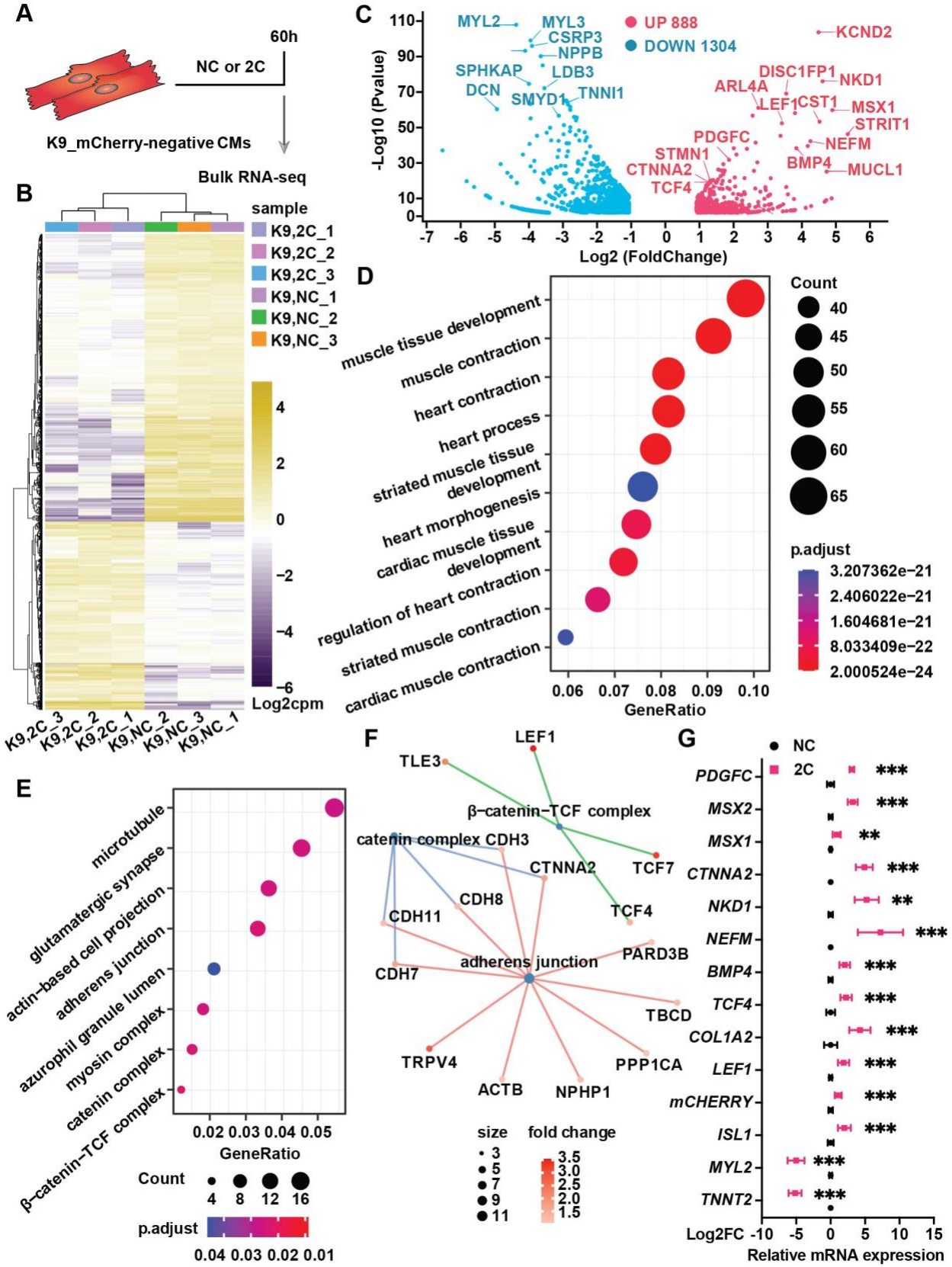
A
60h
NC or 2C
K9_mCherry-negative CMs
Bulk RNA-seq
B
sample
K9,2C_1
K9,2C_2
K9,2C_3
K9,NC_1
K9,NC_2
K9,NC_3
Log2cpm
C
UP 888
DOWN 1304
-Log10 (Pvalue)
Log2 (FoldChange)
MYL2
MYL3
CSRP3
NPPB
SPHKAP
LDB3
DCN
SMYD1
TNNI1
KCND2
DISC1FP1
NKD1
ARL4A
LEF1
CST1
MSX1
STRIT1
PDGFC
NEFM
STMN1
BMP4
CTNNA2
MUCL1
TCF4
D
muscle tissue development
muscle contraction
heart contraction
heart process
striated muscle tissue development
heart morphogenesis
cardiac muscle tissue development
regulation of heart contraction
striated muscle contraction
cardiac muscle contraction
GeneRatio
Count
p.adjust
E
microtubule
glutamatergic synapse
actin-based cell projection
adherens junction
azurophil granule lumen
myosin complex
catenin complex
β-catenin-TCF complex
GeneRatio
Count
p.adjust
F
LEF1
TLE3
β-catenin-TCF complex
catenin complex CDH3
CTNNA2
TCF7
CDH8
TCF4
CDH11
adherens junction
PARD3B
CDH7
TBCD
TRPV4
PPP1CA
ACTB
NPHP1
size
fold change
G
NC
2C
PDGFC
MSX2
MSX1
CTNNA2
NKD1
NEFM
BMP4
TCF4
COL1A2
LEF1
mCHERRY
ISL1
MYL2
TNNT2
Log2FC
Relative mRNA expression

465

Fig. 6. Single-cell RNA-seq of 2C-treated mCherry-negative CMs. A, UMAP analysis showing 7 clusters in cells induced from K9-derived mCherry-negative CMs by treatment with DMSO (NC) and 2C for 60 hours. **B,** The percentage of cells in the 7 indicated clusters, following DMSO (NC) or 2C treatment. **C,** Heatmap showing the differentially expressed genes in the cells from 7 indicated clusters. The representative marker genes of 7 indicated clusters were listed on the right. **D,** Violin plots showing the expression levels of marker genes of CMs (MYL2, MYH6), ICs (COL1A1, ACTA2), and RCCs (ISL1, BMP4, FGF20) among cells from 7 indicated clusters. **E,** UMAP analysis showing the second-level clustering of cluster 2 into 4 subclusters (left), which exhibited dramatic distinction under condition of 2C or NC (right). **F,** The percentage of cells in the 4 indicated subclusters within cluster 2, following DMSO (NC) or 2C treatment. **G,** Heatmap showing the differentially expressed genes among cells from 4 subclusters of cluster 2. Genes related to RCCs are highlighted in the green blocks on the right. (**H** and **I**) Pseudotime trajectory showing changes across various cell states upon 2C treatment, which were presented with different developmental pseudotime points (**H**) and cell states (**I**). **J,** Curves showing the dynamic expression of representative genes of RCCs (ISL1, FGF20), ICs (COL1A1), and CMs (TNNT2) along indicated pseudotime points.

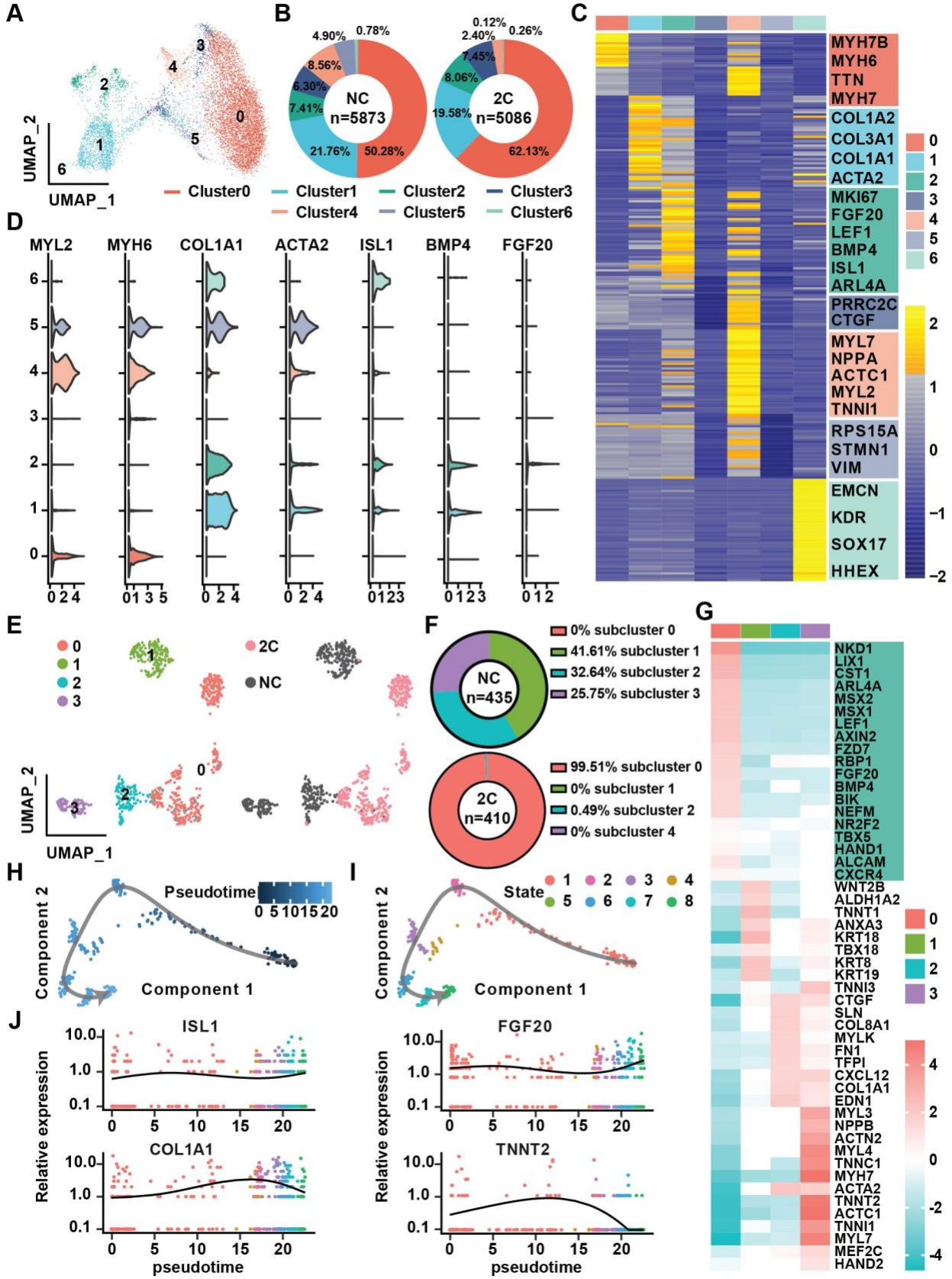
A
UMAP_2
UMAP_1
Cluster0
Cluster1
Cluster2
Cluster3
Cluster4
Cluster5
Cluster6
B
NC
n=5873
2C
n=5086
C
MYH7B
MYH6
TTN
MYH7
COL1A2
COL3A1
COL1A1
ACTA2
MKI67
FGF20
LEF1
BMP4
ISL1
ARL4A
PRRC2C
CTGF
MYL7
NPPA
ACTC1
MYL2
TNNI1
RPS15A
STMN1
VIM
EMCN
KDR
SOX17
HHEX
D
MYL2
MYH6
COL1A1
ACTA2
ISL1
BMP4
FGF20
E
2C
NC
F
NC
n=435
0% subcluster 0
41.61% subcluster 1
32.64% subcluster 2
25.75% subcluster 3
2C
n=410
99.51% subcluster 0
0% subcluster 1
0.49% subcluster 2
0% subcluster 4
G
NKD1
LIX1
CST1
ARL4A
MSX2
MSX1
LEF1
AXIN2
FZD7
RBP1
FGF20
BMP4
BIK
NEFM
NR2F2
TBX5
HAND1
ALCAM
CXCR4
WNT2B
ALDH1A2
TNNT1
ANXA3
KRT18
TBX18
KRT8
KRT19
TNNI3
CTGF
SLN
COL8A1
MYLK
FN1
TFPI
CXCL12
COL1A1
EDN1
MYL3
NPPB
ACTN2
MYL4
TNNC1
MYH7
ACTA2
TNNT2
ACTC1
TNNI1
MYL7
MEF2C
HAND2
H
Pseudotime
Component 2
Component 1
I
State
J
ISL1
COL1A1
FGF20
TNNT2
Relative expression
pseudotime

481

Fig. 7. Chromatin immunoprecipitation-sequencing (ChIP-seq) analyses of chemical-treated H9 hESC-derived CMs. A, Schematic illustration of ChIP-seq analysis of H9-derived CMs subjected to DMSO, A-485, CHIR99021, or 2C treatment for 60 hours. **B,** Average ChIP-seq signal profiles showing the indicated histone modifications around the TSS in the input and ChIP samples prepared from DMSO and 2C-treated cells. **C,** Heatmap showing the whole-genome wide distribution of H3K9Ac, H3K27Ac, and H3K4me3 peaks within a range of ±4kb from TSSs in the cells treated with DMSO or 2C for 60 hours. **D,** H3K9Ac and H3K27Ac peaks surrounding CM genes (TNNT2 and TNNI1) and RCC genes (LEF1 and ISL1) in the cells treated with DMSO, A-485, CHIR99021 or 2C for 60 hours, and H3K4me3 peaks surrounding the same genes in the cells treated by DMSO or 2C. **E,** Veen diagram showing the number of annotated genes with H3K9Ac or H3K27Ac enrichment in the cells treated with DMSO, A-485, CHIR99021 or 2C for 60 hours. Red circles indicate the number of genes with unique H3K9Ac or H3K27Ac enrichment induced by 2C treatment; black circles indicate the number of genes with H3K9Ac or H3K27Ac enrichment unaffected by any chemical treatment. (**G**-**J**) The annotated genes with the most significant changes in H3K9Ac enrichment following treatment with DMSO (**G**) or 2C (**I**) were ranked by Log10LR and analyzed by GOs (**H** and **J**), respectively. **K,** ISL1 binding motifs identified from the cells treated with A-485 or 2C.

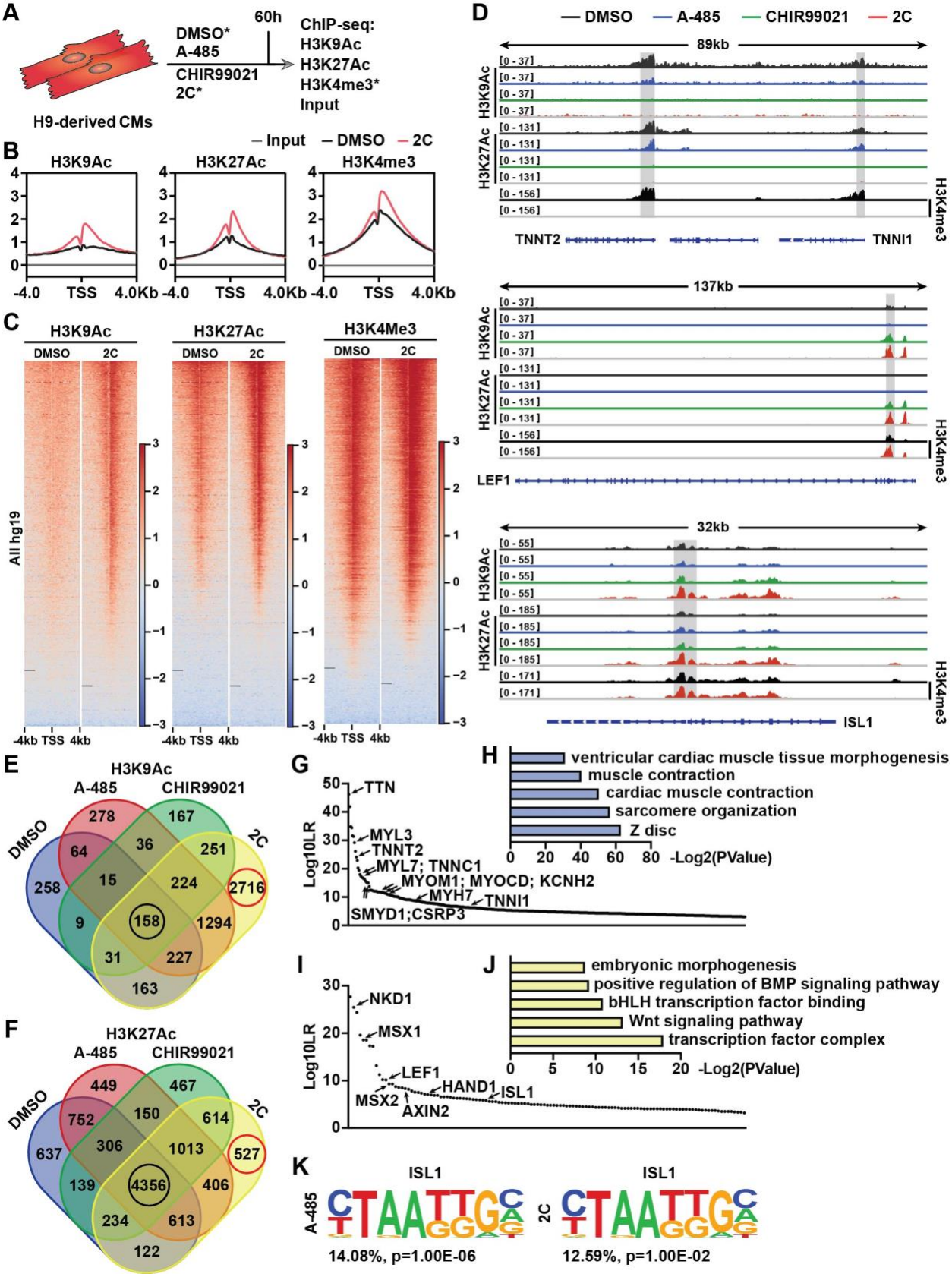
A
H9-derived CMs
DMSO*
A-485
CHIR99021
2C*
60h
ChIP-seq:
H3K9Ac
H3K27Ac
H3K4me3*
Input
B
Input
DMSO
2C
H3K9Ac
H3K27Ac
H3K4me3
-4.0
TSS
4.0Kb
C
H3K9Ac
H3K27Ac
H3K4Me3
DMSO
2C
All hg19
-4kb TSS 4kb
D
DMSO
A-485
CHIR99021
2C
89kb
H3K9Ac
H3K27Ac
H3K4me3
TNNT2
TNNI1
137kb
LEF1
32kb
ISL1
E
H3K9Ac
A-485
CHIR99021
DMSO
2C
278
167
64
36
251
258
15
224
2716
9
158
1294
31
227
163
F
H3K27Ac
A-485
CHIR99021
DMSO
2C
449
467
752
150
614
637
306
1013
527
139
4356
406
234
613
122
G
Log10LR
TTN
MYL3
TNNT2
MYL7; TNNC1
MYOM1; MYOCD; KCNH2
MYH7
TNNI1
SMYD1;CSRP3
H
ventricular cardiac muscle tissue morphogenesis
muscle contraction
cardiac muscle contraction
sarcomere organization
Z disc
-Log2(PValue)
I
Log10LR
NKD1
MSX1
LEF1
HAND1
ISL1
MSX2
AXIN2
J
embryonic morphogenesis
positive regulation of BMP signaling pathway
bHLH transcription factor binding
Wnt signaling pathway
transcription factor complex
-Log2(PValue)
K
A-485
ISL1
14.08%, p=1.00E-06
2C
ISL1
12.59%, p=1.00E-02